

Number counts and redshift distribution of gravitational arclets as a probe of galaxy evolution

J. Bézecourt, R. Pelló, G. Soucail

Observatoire Midi-Pyrénées, Laboratoire d'Astrophysique, UMR 5572, 14 Avenue E. Belin, F-31400 Toulouse, France

Received, Accepted

Abstract. We present a detailed model of the absolute number counts, color and redshift distributions of gravitational arclets observed in clusters of galaxies. The framework adopted for galaxy evolution is chosen to fairly reproduce the observed number counts and redshift distribution of field galaxies. Then, the spectrophotometric evolutionary code is coupled with an accurate modelling of the cluster-lens mass distribution. The interest in applying these calculations to arclets is to use cluster-lenses as filters to select faint distant galaxies. This procedure is applied on two different cluster-lenses, Abell 2218 and Abell 370, for which the mass distribution is well constrained. We have studied the impact of the different sources of uncertainty on the predicted number counts and redshift distributions, taking into account the observational conditions for two sets of data, HST and ground-based images. We investigate in details the influence of the mass modelling on the counts and we show that simple cluster-scale potentials can no longer be used for arcs statistics. The main result is that arcs at redshifts between 0.5 and 1 are correctly predicted by the modelling as observed. Nevertheless, an important population of high redshift arclets ($z \geq 1.0$) is also revealed by the simulations, which is not observed in spectroscopic surveys of arclets. We discuss the nature of this disagreement, probably due to uncertainties in the evolutionary models adopted here for galaxies at high redshift. The spatial distribution of arclets in number density and the local mean redshift of the sample are also derived. These maps can be used as a tool to optimize the search for high redshift galaxies magnified by the clusters of galaxies.

Key words: Galaxies: cluster: individual: Abell 370, Abell 2218 – Galaxies: evolution – Cosmology: observations – gravitational lensing

1. Introduction

The measure of galaxy number counts and the study of the spectrophotometric properties of faint galaxies are probably the two leading topics to constrain the evolutionary history of galaxies, a point which is absolutely needed in cosmology. The new observational tools coming from HST imagery surveys, deep number magnitude counts in different wavelengths and spectroscopic surveys of faint galaxies have allowed to approach the spectromorphological evolution of galaxies in a reliable way. For the first time, some clues have been proposed to explain the nature of the faint blue galaxies and to determine the star formation history (see the review by Koo and Kron 1992 and Ellis 1997). Nevertheless, it is still difficult to estimate the rate at which this evolution occurs as well as the physical processes involved, because number counts are integrated values over the redshift distribution and the luminosity distribution of galaxies. Spectroscopic surveys in deep fields are one of the issues to treat the problem, but they are limited in magnitude. For example, the surveys up to the limit $B = 24$ (Glazebrook et al. 1995, Cowie et al. 1996) show a peak at $z \simeq 0.5 - 0.7$, but the lack of a large number of high redshift objects in these surveys argues for a mild luminosity evolution at intermediate redshift. From a deep sample of I -band selected galaxies, the Canada France Redshift Survey (CFRS, Lilly et al. 1995) reveals an evolution in the luminosity function (LF) of the bluer field galaxies of about 1 magnitude between $z = 0.7$ and $z = 0$ but again fails to identify a population of high- z galaxies. Spectroscopic data acquired by the Autofib Redshift Survey (Ellis et al. 1996) leads to similar conclusions about the evolution of the luminosity function with redshift and show also a clear steepening in the faint end slope of the LF.

A powerful way to investigate higher redshifts with the same magnitude limit is possible thanks to the gravitational magnification of background sources in the field of massive clusters of galaxies (see Fort and Mellier 1994 for a review). Serendipitously lensed by a foreground cluster, gravitational arcs and arclets are representative

of a rather distant population of galaxies, at least up to a redshift ~ 1 (Soucail et al. 1988, Pelló et al. 1991, Bézecourt and Soucail 1997, Ebbels et al. 1997), or even higher in a few cases (Mellier et al. 1991, Ebbels et al. 1996). But again the magnitude limitation for spectroscopy prevents an extensive and deep analysis. Photometric identification of very high redshift objects has also proved very successful in the case of multiple images lensed by a massive cluster of galaxies (Trager et al. 1997, Frye & Broadhurst 1997, Pelló et al. 1997). To overcome the difficulty, several approaches are proposed, each of them being based on a redshift estimate for individual arclets. A promising one is the lens inversion technique which consists in finding the most probable redshift for each arclet depending on its location and shape parameters for a given lens model of the cluster potential (Kneib et al. 1994a, Kneib et al. 1996, Ebbels et al. 1997). Successfully used in a few cases, it allows to reach intrinsic magnitudes up to $B \simeq 27$. The redshift distribution of gravitational arclets can also be estimated with multicolor photometry (Pelló et al. 1996), thanks to the photometric redshift estimated from a long wavelength baseline (from U to K). A more straightforward method consists in measuring the depletion in counts of arclets caused by the amplification bias: depending on the slope of the field galaxies number counts, the radial density of arclets will show a depletion curve characteristic of the sources redshift (Broadhurst 1995, Fort et al. 1996). The drawing of the critical lines corresponding to the most distant galaxies was also proposed as a sub-product of this method and could be used to constrain the redshift of formation of the galaxies.

The aim of the paper is to probe the spectrophotometric evolution of galaxies by computing both the number counts of arclets behind a cluster-lens and their redshift distribution. The basic idea is to consider cluster-lenses as “high- z filters” which select background galaxies and distort them, making their shape easier to identify. So the sample of arclets is a subsample of a global sample of faint field galaxies in which galaxy evolution at relatively large look-back times may be much stronger. The deep number counts of arclets are then supposed to probe more directly the redshift distribution of *distant* galaxies and their relative weight with respect to a possible population of faint nearby galaxies. Previous statistical studies about the occurrence rate of arcs or arclets assumed spherical potential for all clusters and/or neglected galaxy evolution (Nemiroff and Dekel 1989, Smail et al. 1991, Wu and Hammer 1993, Grossman and Saha 1994, Smail et al. 1994, Refregier and Loeb 1997, Hattori et al. 1997). The authors were more concerned about constraining the mass profile of the lenses, whereas in this paper we want to emphasize the implications on galaxy evolution. For this reason, we apply our models on real cluster-lenses (Abell 370 and Abell 2218) for which the presence of multiple-images

strongly constrains the potential in the cluster core. Moreover in order to optimise the arclets identification among the crowded cluster fields, we use deep HST images available for both clusters.

This paper is organised as follows: in Section 2, we compute the number counts of gravitational arclets by combining models of spectrophotometric evolution of galaxies, which reproduce the field number-counts, and realistic models of mass distribution for clusters, which are well constrained by multiple images and giant arcs. The sensitivity of our model with respect to uncertainties on the lensing potential at large radii is tested, and the robustness of the results with respect to some observational criteria such as axis ratio or surface brightness is explored. Section 3 presents the results obtained with this method on two cluster-lenses, A2218 and A370, including a comparison between the predicted number counts of arclets and the observed ones. The sensitivity of our model to different parameters is discussed in Section 4, and some clues about the possibility to detect high- z galaxies are also considered. Finally, conclusions are presented in Section 5.

Throughout the paper, we consider a Hubble constant of $H_0 = 50 \text{ km s}^{-1} \text{ Mpc}^{-1}$, with $\Lambda = 0$.

2. Number counts and redshift distribution of gravitational arclets

The surface density of gravitational arclets obeys to two competing effects: one is the magnification of the luminosity by the cluster potential and the other one is surface dilution. If $n(< m) = n_0 10^{\alpha m}$ is the surface density of galaxies up to magnitude m with slope α , the density of arclets magnified by a factor M is

$$n_{arc}(< m) = \frac{1}{M} n(< m + 2.5 \log M) \quad (1)$$

Hence,

$$\frac{n_{arc}(< m)}{n(< m)} = M^{2.5\alpha - 1} \quad (2)$$

The dominating effect depends on the slope of number counts in empty fields without magnification by an intervening mass. For steep counts ($\alpha > 0.4$), gravitational lensing will increase the surface density whereas for shallower counts a depletion will take place (Broadhurst 1995, Fort et al. 1996).

Looking in details at the number counts behind a cluster-lens, we can write the number of arclets brighter than magnitude m with an axis ratio greater than A_{min} and a surface brightness brighter than μ_0 within a given region of the sky as:

$$N(m, A_{min}, \mu_0) = \sum_i \int_{z_l}^{z_{max}} \int_{A_{min}}^{\infty} S(A, z) dA \int_{L_{min}}^{L_{max}} \Phi_i(L, z) dL \frac{dV}{dz} dz \quad (3)$$

The summation is over the different morphological types and z_l is the lens redshift. $z_{max}(\mu_0, i)$ is the redshift cut-off corresponding to the limit in central surface brightness μ_0 . $S(A, z, H_0, \Omega)$ is the angular area in the source plane (at redshift z) filled by sources corresponding to arclets with an axis ratio between A and $A + dA$. $\Phi_i(L, z)$ is the LF at redshift z for each morphological type. $L_{min}(z, m, A, H_0, \Omega)$ is the luminosity of an object at redshift z which has an apparent magnitude m after magnification by the cluster, assuming that the source is circular and that its axis ratio is A after magnification (see below in §2.3). Finally, L_{max} is the bright end of the LF and $dV(z, H_0, \Omega)$ is the volume element.

The main differences with standard number counts are: firstly, the integration in redshift runs from the lens-redshift z_l as a minimum up to a limit which depends essentially on the limitation in surface brightness $z_{max}(\mu_0, i)$. Gravitational lensing preserves the surface brightness of the sources, so a cut in observed surface brightness is more realistic than a cut in magnitude for extended objects. Secondly, one has to take into account the differential observed surface, computed in the source plane for each redshift and for each magnification. Finally, each luminosity has to be corrected from the magnification before the integration over the LF of the sources, as well as the minimum limit in luminosity. An additional application is to compute local values of the different parameters to derive the 2D projected number density and the mean redshift of arclets (see §3.6).

In order to validate this computation of number counts, we check first in the following section that observations in empty fields are correctly reproduced by the evolution model. We then present how to include a mass model in the problem, and the way both models are combined. We finally investigate the sensitivity of counts to these mass distributions.

2.1. Number counts and redshift distribution of field galaxies

2.1.1. Spectral energy distributions for template galaxies

As a first step, one has to define a framework for galaxy evolution that fairly reproduce both the number counts and the redshift distribution of field galaxies. We follow here the results of Pozzetti et al. (1996, hereafter PBZ) using the Bruzual and Charlot evolutionary code (1993 updated as GISSEL95). Four galaxy types are used to represent the distribution in morphological types. They correspond respectively to an exponential star formation rate (SFR) for elliptical and spiral galaxies, with time scales of 1 Gyr and 10 Gyr for $q_0 = 0$ (model 1) and 1 Gyr and 8 Gyr for $q_0 = 0.5$ (model 2). A constant SFR is assumed for late type galaxies and a population of eternally young objects is also introduced by the authors to account for very blue objects. The redshift of formation for all galax-

ies is $z_{form} = 4.5$ for model 1 and 5 for model 2. It should be noted that an additional assumption is made in PBZ by considering different initial mass functions for late type spirals (Salpeter IMF, Salpeter 1955) with respect to ellipticals and normal spirals (Scalo IMF, Scalo 1986). This is necessary to obtain good fits to number counts from U -band to K -band, although the predicted colors for nearby galaxies does not match very well those observed and appear too red. A better agreement would require the use of a Salpeter IMF for all types but the drawback is that too many high redshift galaxies are produced, compared to spectroscopic surveys. Being aware of this discrepancy we choose as prime constraints number counts and redshift distribution of field galaxies and adopt the same parameters as PBZ. A summary of the ingredients of our models is presented in Table 1. The colors for the different galaxy types at $z = 0$ are given in Table 2, and compared to those observed in the local universe or directly derived from observed spectra (Fukugita et al. 1995).

2.1.2. Luminosity function

The weight affected to each galaxy type is taken from the determination of the local LF by Efstathiou et al. (1988), with the assumption that (1) morphological types are equivalent to spectroscopic types at any redshift, and (2) the weights of spectromorphological types remain unchanged with z . A model fulfilling these two conditions is a pure luminosity evolution model. Moreover, density evolution can occur due to the addition of a population of dwarf objects at low redshift or to an earlier phase of merging. A change in the overall density is not required in a low Ω universe but it is necessary in a closed universe to reproduce number counts (Rocca-Volmerange and Guiderdoni 1990, Broadhurst et al. 1992). We consider here two different models, which correspond to these two cases:

- Model 1: $q_0=0$, with a constant Schechter function, which is a pure luminosity evolution model.
- Model 2: $q_0=0.5$, a number luminosity evolution model which keeps constant the comoving mass density. The LF evolves with z according to the merging law of Rocca-Volmerange and Guiderdoni (1990):

$$\Phi_i(L, z) = (1+z)^{2\eta} \Phi_i(L(1+z)^\eta, z=0) \quad (4)$$

where

$$\Phi_i(L, z=0)dL = \Phi_i^* \left(\frac{L}{L_*(i)} \right)^{\alpha(i)} e^{-\frac{L}{L_*(i)}} \frac{dL}{L_*(i)} \quad (5)$$

is the LF at $z = 0$ described by a Schechter law. i corresponds to each morphological type and $\eta = 1.5$ is adjusted by Rocca-Volmerange and Guiderdoni to reproduce the field number counts. Φ_i^* is the normalisation of the LF for each morphological type (Table 1). In the integration over the luminosities, we stop the bright end of the blue LF at $M_{Bmax} = -23.5$ for any z in model 1, and at $L_{Bmax}(z) = L_{Bmax}(z=0)/(1+z)^\eta$ with $L_{Bmax}(z=0)$ corresponding to $M_{Bmax} = -23.5$ for model 2.

Table 1. Ingredients of the two number counts models, for two selected cosmologies.

| model | q_0 | Spectral type | fraction % | SFR | IMF | z_f | density evolution | Φ_i^* $10^{-3} h_{50}^3 Mpc^{-3}$ | α | M_{B^*} |
|-------|-------|---------------|------------|---------------------|----------|-------|-------------------|---|----------|-----------|
| 1 | 0 | E/S0 | 0.28 | exp. $\tau = 1Gyr$ | Scalo | 4.5 | no | 0.95 | -0.48 | -20.87 |
| | | Sab/Sbc | 0.47 | exp. $\tau = 10Gyr$ | Scalo | | | 1.15 | -1.24 | -21.14 |
| | | Scd/Sdm | 0.22 | constant | Salpeter | | | 0.54 | -1.24 | -21.14 |
| | | vB | 0.03 | | Salpeter | | | 0.12 | -1.24 | -21.14 |
| 2 | 0.5 | E/S0 | 0.28 | exp. $\tau = 1Gyr$ | Scalo | 5 | yes | 0.95 | -0.48 | -20.87 |
| | | Sab/Sbc | 0.47 | exp. $\tau = 8Gyr$ | Scalo | | | 1.15 | -1.24 | -21.14 |
| | | Scd/Sdm | 0.22 | constant | Salpeter | | | 0.54 | -1.24 | -21.14 |
| | | vB | 0.03 | | Salpeter | | | 0.12 | -1.24 | -21.14 |

Table 2. Colors of model and observed galaxies (Fukugita et al. 1995).

| type | $U - B$ | | | $B - V$ | | | $V - I$ | | |
|---------|-----------|-------------|-----------|-----------|-------------|-----------|-----------|-------------|-----------|
| | $q_0 = 0$ | $q_0 = 0.5$ | observed | $q_0 = 0$ | $q_0 = 0.5$ | observed | $q_0 = 0$ | $q_0 = 0.5$ | observed |
| E/S0 | 0.70 | 0.63 | 0.45/0.40 | 0.99 | 0.96 | 0.97/0.93 | 1.61 | 1.56 | 1.45/1.25 |
| Sab/Sbc | 0.22 | 0.19 | 0.13 | 0.68 | 0.65 | 0.73 | 1.33 | 1.29 | 1.30 |
| Scd/Sdm | -0.12 | -0.14 | -0.11 | 0.43 | 0.41 | 0.43 | 1.13 | 1.10 | 1.17 |
| vB | -0.61 | -0.61 | — | 0.01 | 0.01 | — | 0.62 | 0.62 | — |

Model 2 produces more faint objects at high redshift than model 1, a trend which is consistent with the results of the Autofib Redshift Survey (Ellis et al. 1996). Nevertheless, this qualitative model is somewhat unrealistic because the photometric properties induced by merging are not investigated in details. In any case, model 2 is a useful approach to the $q_0 = 0.5$ scenario in view of the high M/L values found in weak lensing analysis (see Narayan and Bartelmann 1996 for a review) which seem to reject a low Ω universe. Finally, the number counts of arcs and arclets are limited to redshifts higher than the lens redshift, and they are mainly sensitive to rather bright objects, even at the faintest magnitudes. For this reason, these counts do not depend severely on the uncertainties on the faint end slope of the local LF.

2.1.3. Surface brightness

As the detection of extended objects is highly dependent on surface brightness, we include this effect in the models. We assign a gaussian distribution of central surface brightness in B (μ^0) to each morphological type. The parameters defining these observed distributions in the local universe have been taken from the literature (all the units are in $mag/''^2$):

- E: $\langle \mu^0 \rangle = 17.55$, $\sigma = 0.15$ (King 1978)

- S0, Sa, Sb and Sc: $\langle \mu^0 \rangle = 21.02$, $\sigma = 0.42$ (Van der Kruit 1987)
- Sd and Im: $\langle \mu^0 \rangle = 22.24$, $\sigma = 0.49$ (Van der Kruit 1987)

The evolution of μ^0 with z obeys to the standard relationship:

$$\mu^0(z) = \mu^0(z=0) + k(z) + e(z) + 2.5 \log(1+z)^4 \quad (6)$$

where $k(z)$ and $e(z)$ are computed with the Bruzual & Charlot code. When no other value is indicated, the surface brightness limit for the detection is $28 \text{ mag}/''^2$ in B , a value which is close to the 2σ detection level in most cases considered here. At redshift z and for each morphological type and magnitude, a visibility weight is introduced according to the above surface brightness distributions to compute the total fraction of objects actually detected.

On ground-based images, the seeing spreads the light coming from the center of the objects. For number counts of arcs and arclets, the effect of seeing is also important because it modifies the shapes of the images (see details in §2.3 and §2.4). Several effects should be considered to properly take into account the results of seeing on galaxy profiles and to include an observational cut in surface brightness. In principle, the luminosity profile for each morphological type defines a characteristic radius which is related to the total luminosity of the galaxy, $L(z)$. This

characteristic angular radius θ is then convolved with the seeing to give an *observed* central surface brightness μ_{obs}^0 . A cut in μ_{obs}^0 induces a maximum redshift at which the galaxy can be observed. This effect is minor for elliptical galaxies because $z_{cut} > z_{form}$ provided that the surface brightness limit is faint enough, but it should be much more sensitive for spirals. We have adopted here the crude weighting described above, as a function of μ_{obs}^0 , and the selection is often performed on WFPC HST images, where these seeing effects are negligible in practice. A more realistic treatment of source profiles will require a fair knowledge of the morphological evolution of galaxies, taking into account that morphology is expected to be strongly wavelength dependent.

2.1.4. Results

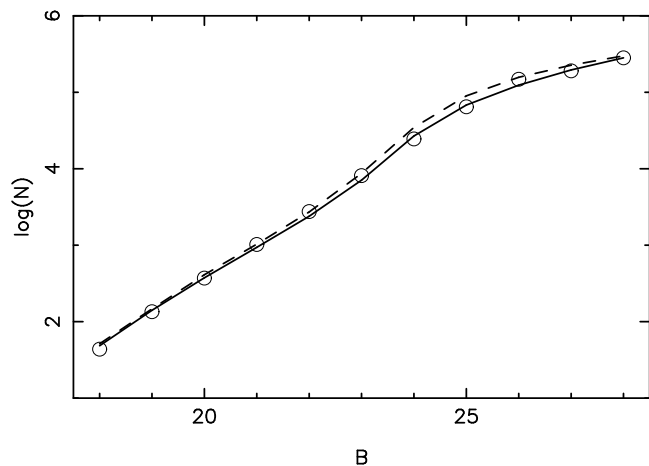


Fig. 1. Observed blue number counts (\circ) (from the compilation by Metcalfe et al. (1991) completed by Williams et al. (1996)) and counts derived by the model for model 1 (dashed line) and model 2 (solid line) per bin of one magnitude and per square degree.

The predictions of field number counts in the B -band are presented in Figure 1, and the corresponding redshift distributions are shown in Figure 2. All these calculations were performed without seeing. Observed number counts are taken from the compilation by Metcalfe et al. (1991) of various works. The counts at faint magnitudes were obtained by Williams et al. (1996) from the Hubble Deep Field survey. When we introduce a seeing of $0''.8$ and a more accurate treatment of galaxy profiles, only a slight difference appears for the faintest bin in magnitude, where the counts are reduced to $\sim 80\%$ of their value without seeing.

We also checked that number counts in filters U and I were correctly reproduced as well as the redshift distribution of galaxies selected in I ($17 < I < 22$) according to the CFRS (Crampton et al. 1995). Infrared counts in the

K -band are somewhat more discrepant and show an underestimate of the counts predicted at faint magnitudes.

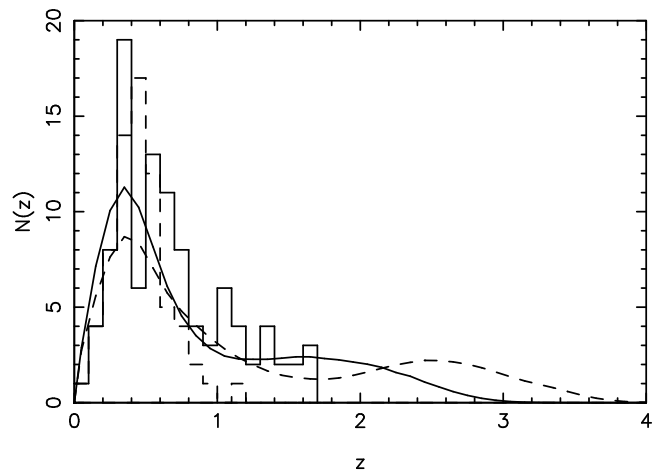


Fig. 2. Redshift distribution of galaxies with $22.5 \leq B \leq 24$ for model 1 (dashed line) and model 2 (solid line). Numbers are absolute counts per bin of 0.1 in redshift, normalized to the total counts by Cowie et al. (1996). The solid histogram is from Cowie et al. (1996) data and the dashed histogram is from Glazebrook et al. (1995). Models predict $\sim 20\%$ of the total number counts at $z \geq 1.5$,

2.2. Mass distributions in clusters lenses

An accurate modelling of the mass distribution in the lens is needed because, in principle, any variation in the local substructures or in the slope of the potential may induce a change in the local magnification and axis ratio of the background galaxies. Steep surface mass density profiles will produce arclets narrower than a more gradual slope (Hammer 1991). For this reason, the model is applied in the first place to two well studied cluster-lenses, using the published lens models: A370 at $z = 0.375$ (Kneib et al. 1993) and A2218 at $z = 0.176$ (Kneib et al. 1995, Kneib et al. 1996). Both clusters are very well represented by bimodal cluster-scale mass distributions, with the clumps being centered on the two main galaxies and the potentials modelled by pseudo isothermal elliptical distributions (PIEMD, Kassiola and Kovner 1993). In the improved modelling for A2218 (Kneib et al. 1996), the authors introduce an additional galaxy-scale component in the mass distribution. Each one of the 34 brightest cluster galaxies is modelled by a pseudo-isothermal elliptical mass distribution with the parameters (truncation radius, core radius and velocity dispersion) scaled to the galaxy luminosity. The effect on number counts of uncertainties in the mass distribution is quantified below (see §2.5).

2.3. Axis ratio and magnification

The axis ratio of an arclet is the result of the intrinsic size of the source, tangential and radial magnifications and seeing. The images from the Medium Deep Survey (the MDS project) show that the intrinsic size of galaxies seems rather constant until $z \simeq 0.8$ (Mutz et al. 1994). On the contrary, the results of lens inversion based on HST images (scanning higher redshift galaxies) lead to the conclusion that the half light radius of the sources of giant gravitational arcs is decreasing with increasing redshift following approximately the law $r_{hl} \propto 1/(1+z)$ (Smail et al. 1996). This effect is relevant in the merging hypothesis and implies lower dimensions for high redshift objects. We include the decreasing law as an additive hypothesis in models 1b and 2b, for $q_0 = 0$ and $q_0 = 0.5$ respectively. The evolution of the linear size then follows the relation

$$r_{hl} = \frac{8.7}{1+z} \text{kpc} \quad (7)$$

scaled with the average half light radius of nearby spiral galaxies (8.7 kpc, Mathewson et al. 1992), and also in good agreement with the typical sizes observed for the most distant galaxies (Trager et al. 1997, Lowenthal et al. 1997). Models 1a and 2a are the equivalent ones with a constant linear size of 8.7 kpc, whatever the redshift.

All sources are considered circular because it is not worth introducing an ellipticity distribution when we are only interested in arclets with rather high axis ratio ($a/b \geq 2$), and when the intrinsic ellipticity of sources is negligible compared to the one induced by the lens. However, we are aware of the higher importance of source ellipticities in weak lensing studies, when reconstructing mass profiles. Hence the observed axis ratio is:

$$\frac{a}{b} = \sqrt{\frac{(2\lambda_t\theta_{hl})^2 + s^2}{(2\lambda_r\theta_{hl})^2 + s^2}} \quad (8)$$

λ_t and λ_r being the tangential and radial magnification, θ_{hl} the half light angular radius and s the seeing or the width of the PSF.

$S(A, z)$ in equation 3 is the background surface at redshift z where the sources have an axis ratio between A and $A + 1$ after magnification. It is a specific term related to lensing and magnification, which makes the arclet number counts quite different from results in empty fields. Numerically, $S(A, z)$ is obtained by computing the area in the image plane where arclets with $A \leq a/b \leq A + 1$ can be found, and then dividing by the magnification at each point because of the dilution factor in the image plane. The upper limit chosen for the magnification is 20, a value representative of giant arcs, but of negligible effect because statistics is not dominated by giant arcs. In practice, as number counts will be computed in the image plane, we have chosen to scan this plane with a grid of $1''$ step and then to relate these image elements to the corresponding surface in the source plane at each redshift.

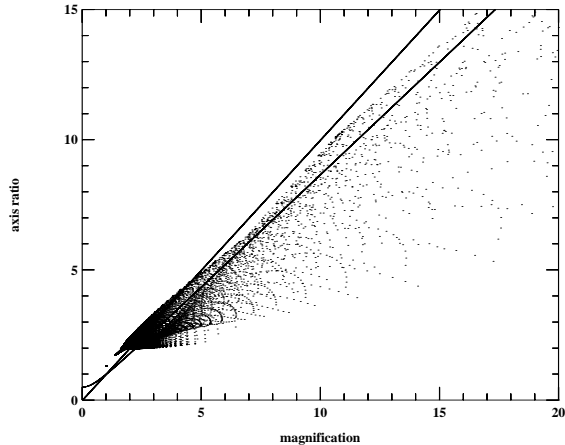


Fig. 3. Axis ratio versus magnification expected in the field of the HST image for background galaxies at $z=0.8$ lensed by the cluster A2218, using the lens modelling by Kneib et al. (1995) and our model 1 (dots). For comparison, the same relation is displayed for a SIS potential with $\lambda_r = 1$, with and without a seeing of $1''$ (lower and upper lines respectively). In ideal conditions, without either seeing or pixel sampling, magnification and axis ratio are equal for a SIS.

In the case of a circular potential, two arclets at the same redshift with the same axis ratio would have identical magnifications. But the link between the axis ratio and the magnification of an arclet is not unique in the more realistic cases considered in this paper (bimodal potentials, perturbing galaxies). Figure 3 illustrates this effect on the relationship between axis ratio and magnification, for a realistic set of parameters in the cluster-lens A2218, compared to the results expected when the potential corresponds to a singular isothermal sphere (SIS). In practice, to compute the intrinsic magnitude of an arclet at redshift z and with an axis ratio between A and $A + 1$, the net magnification by the cluster was assumed to be the averaged magnification factor for all the arclets with the same axis ratio and redshift. The effect of the finite size of sources was neglected when computing magnifications: in regions close to critical lines the magnification of an extended source is different from that of a point source at the same location, it does not grow to infinity. Indeed, for magnifications smaller than 20 this effect is quite negligible.

2.4. Surface brightness effects

In spite of the fact that gravitational lensing does not change the surface brightness, other intervening effects such as atmospheric seeing, optical PSF and pixel sampling tend to modify it. Thanks to the magnification, an arclet appears larger than the equivalent unlensed galaxy, and its luminosity profile is stretched while the central sur-

face brightness remains unchanged. Hence flattening by the seeing is less effective for a lensed object than for its source galaxy. The relevant parameters become the characteristic lengths of the profile along both axis of the arc, enlarged by the convolution with the full PSF. In addition to simple magnification, gravitational lensing makes the detection of faint galaxies easier by increasing their mean surface brightness. This is even more sensitive for ground-based images (with seeing $\sim 1''$) as point sources are much more attenuated by the PSF. This effect can be approximated by considering the change in surface introduced by the seeing:

$$\mu = \mu(\text{no seeing}) - 2.5 \log \frac{ab}{\sqrt{(a^2+s^2)(b^2+s^2)}} \quad (9)$$

where a and b are the semi major and semi minor axis of the arc and s is the seeing FWHM. In the case of HST data, the FWHM is equal to $0.1''$ although data are undersampled by the pixel size. Of course the result is also sensitive to the way a and b are measured, the central part being more circular than the limiting isophote after convolution. We choose here to consider the half light distances in both axis. A more precise treatment is proposed by Hattori et al. (1997) who consider isophotal magnitudes whereas we are concerned here with total magnitudes, less sensitive to detection conditions. In the following we limit the counts to arcs with central surface brightness $\mu_B^0 < 26.5$ or $\mu_R^0 < 25.5$.

2.5. Sensitivity to the mass distribution

We check here the sensitivity of our model to uncertainties on the mass distribution. In particular, we focus on the effects of varying the assumptions for the cluster potential in the two cluster-lenses considered: A2218 and A370.

As explained in §2.2, two lens models are available for the cluster A2218 (Kneib et al. 1995 and Kneib et al. 1996): the first one with only cluster-scale mass components, and the improved one with 34 additional galaxy-scale components in the mass distribution. Both of them reproduce correctly the observed shear pattern. Nevertheless, the second model increases the local magnification and distorts the critical lines in the regions around each lensing galaxy, in such a way that a lensed image located in this area will be divided in 2 or 3 parts whereas the same object would appear as a giant arc with a smoother cluster-scale potential. Hence a higher number of arclets is expected, for a given set of lens parameters (see also Bartelmann et al. 95). An example of such multiplication of arclets is given by the giant arc #359 at redshift $z = 0.702$ (according to the numbering scheme of Le Borgne et al. 1992). Introducing the local magnification by the mass of galaxies #341 and #373 enabled to identify three other images of this object (arcs #328, #337 and #389). This point is quite crucial in our problem because although they do not dominate the arcs counts, multiple images can distort our statistics of small numbers, at

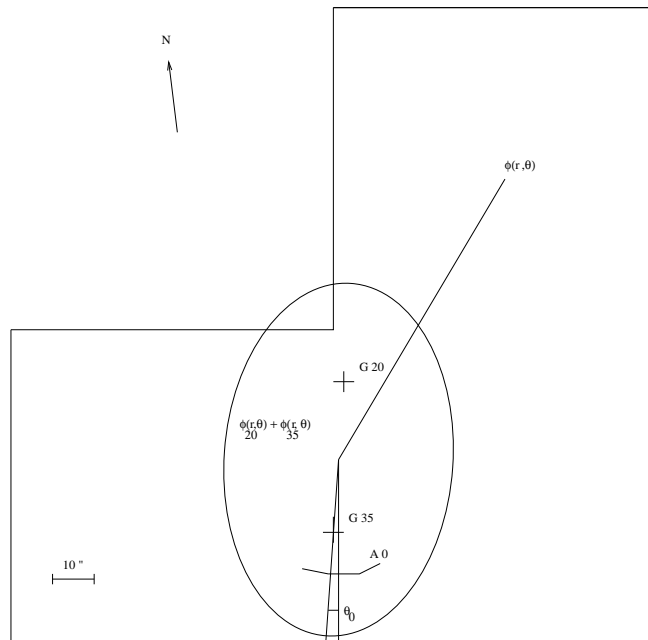


Fig. 4. Field diagram of A370 used in the simulations. The total size is $2.5' \times 2.5'$. The ellipse separates the inner region, where the potential follows the expression of Kneib et al. (1993), from the outer region where the slope is changed to check the dependence of number counts on the shape of the mass distribution.

least in a few magnitude bins. The difference between the expected number counts with these two models, compared to real counts, is shown in Figure 6.

The cluster-scale model of A2218 (Kneib et al. 1995) has been used to investigate the influence of uncertainties in the core radii and the velocity dispersions. To summarize, when these parameters are modified within reasonable values (taking model uncertainties into account), the net result is only a change in the absolute normalisation of $N(z)$, with no shift in the mean redshift of the sample. The results are much more sensitive to errors in velocity dispersions than to core radii. When the core radii varies by 20%, the number of arcs changes by only a 15%, whereas the total number of arclets is modified by 45% for a small change of 10% in the velocity dispersions. It is worth noting that such variations in the parameters are far beyond the published uncertainties.

The uncertainty introduced by the slope of the cluster potential in the external part of the deflector, where most of the arclets appear, has also been investigated with the lens model of A370. In this case, the mass distribution in the central part of the cluster is very well constrained by two systems of multiple images: the giant arc A0 and the pair B2/B3 lead to a bimodal mass distribution with two clumps centered on the cluster galaxies G20 and G35 (Kneib et al. 1993). Hence, we have introduced modifications in the external potential, keeping the center

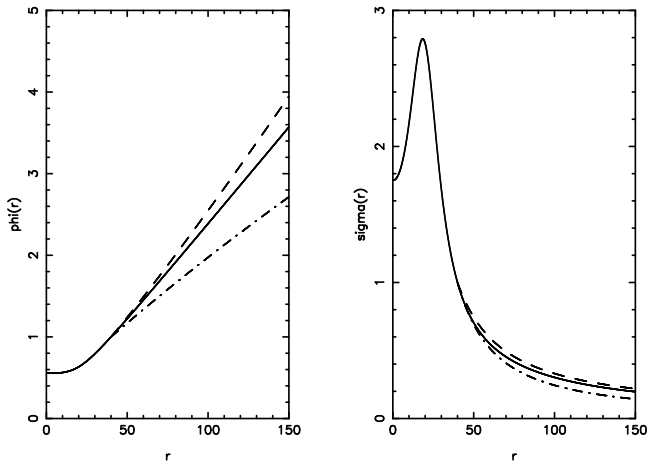


Fig. 5. Gravitational potential (left) and surface mass density (right) along the line G20 – G35 in A370. Solid lines are for the expression given in Kneib et al. (1993); also shown are the cases: $\gamma = 1.1$ (dashed line) and $\gamma = 0.8$ (dot-dashed line).

unchanged. The external region is defined in Figure 4 by an ellipse oriented parallel to the line linking the two central galaxies and with a semi major axis of $40''$. Inside the ellipse we keep the potential to the expression by Kneib et al. (1993)

$$\phi(r, \theta) = \phi_{G20}(r, \theta) + \phi_{G35}(r, \theta) \quad (10)$$

where G20 and G35 are the main cluster galaxies (see Mellier et al. 1988). Outside the ellipse, the potential is not bimodal any longer but it follows the same law as for each clump:

$$\phi(r, \theta) = \phi_0 \left[\sqrt{1 + \left(\frac{r}{r_c}\right)^2} + \frac{\epsilon}{2} \frac{\left(\frac{r}{r_c}\right)^2 \cos(2(\theta - \theta_0))}{\sqrt{1 + \left(\frac{r}{r_c}\right)^2}} \right]^\gamma \quad (11)$$

in polar coordinates, with $\phi_0 = 6\pi \left(\frac{\sigma}{c}\right)^2 r_c \frac{D_{ls}}{D_s}$. θ_0 is the orientation, ϵ the ellipticity, σ the velocity dispersion, r_c the core radius, D_{ls} and D_s are the angular diameter distances respectively between the lens and the source and between the observer and the source. Note that this potential is continuous only along the major axis of the ellipse in Figure 4, but this simplification is only used to test the effects of the slope of the potential on the absolute normalisation of arcs number counts. Outside the ellipse, the parameters of the global potential are $\gamma = 1$, $\epsilon = 0.38$, $r_c = 20''$ and $\sigma = 1000 \text{ km s}^{-1}$ to fit the modelling of Kneib et al. (1993). The values $\gamma = 0.8$ and $\gamma = 1.1$ have been chosen to provide respectively an underestimate and an overestimate of the surface mass density of about 1/3 at large distance from the center of the cluster (Figure 5). Whatever the model used, the change in the amount of mass in the external parts of the cluster-lens simply scales the total number of arcs seen through a cluster, with a negligible change in the mean redshift of the sample (*i.e.* an

overestimate of the total mass, $\gamma=1.1$, increases the number of arclets by 25 % while an underestimate, $\gamma=0.8$, will decrease it by 30 %). More details about the uncertainties induced by the mass modeling are discussed in the next section.

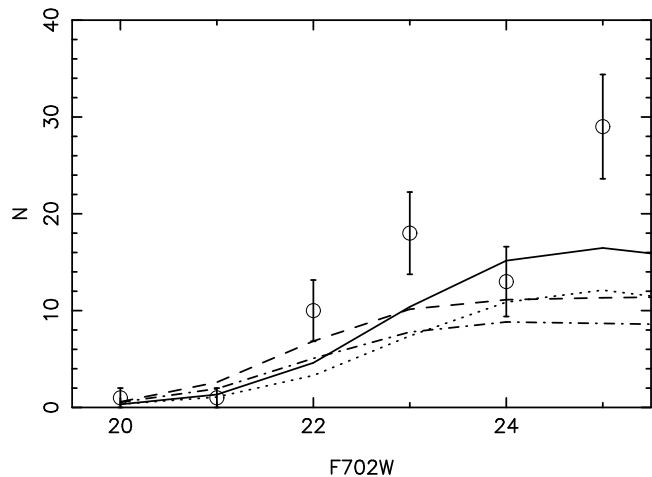


Fig. 6. Number counts of arclets in A2218 with the F702W filter, per bin of one magnitude, up to $R_{F702W}=25$. Selection criteria are: $a/b > 2$ and $\mu_{F702W}^0 \leq 25.5$. \circ : observed counts. The solid line corresponds to $q_0 = 0.5$ (model 2a) and the dashed line to $q_0 = 0.0$ (model 1a), both computed through the lens model by Kneib et al. (1996). The results obtained with the cluster-scale mass distribution only (Kneib et al. 1995) are also displayed for comparison: dotted line and dot-dashed line correspond to count models 2a and 1a respectively. No evolution in the source size has been included as it does not change the graphs (see text for more details). Errors bars correspond to statistical fluctuations.

3. Results

3.1. Catalogs of observed arclets

The detection of arclets in the two cluster-lenses was performed in the frame of WFPC2 HST images, obtained from the STScI Archives: 5600 sec of exposure in filter F675W for A370 (P.I.: R.Saglia), and 6500 sec of exposure in filter F702W for A2218 (Kneib et al. 1996). The $B - F702W$ color distribution of arclets in A2218 is also studied below. Blue magnitudes for A2218 were determined from ground-based deep B images obtained at the 3.5m telescope at Calar Alto (Pelló et al. 1992). The pixel size was $0.25''$ and the seeing was $1.1''$ in this case.

The SExtractor package (Bertin and Arnouts 1996) was used to detect the arclets, with the requirement for an object to have at least 12 contiguous pixels above 2σ of the local sky level. The detection limit at $1\sigma/\text{pixel}$ above the sky is $R \simeq 25.2 \text{ mag}/''^2$ in A2218 and $R \simeq 24.9 \text{ mag}/''^2$ in A370. We limit the sample to objects with total R mag-

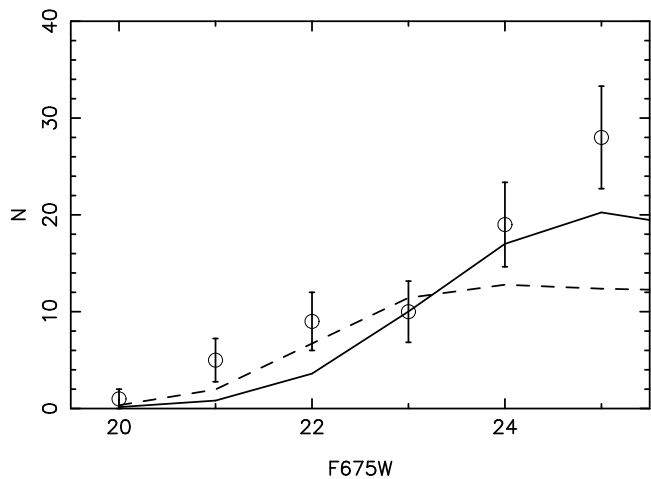


Fig. 7. Number counts of arclets in A370 with the F675W filter, per bin of one magnitude. Selection criteria are: $a/b > 2$ and $\mu_{F675W}^0 \leq 25.5$. Same notations as in Figure 6.

nitude between 21.5 and 25.5 and axis ratio greater than 2, the bright end cut is aimed to avoid contamination by cluster members. A close inspection of each object has been done to eliminate objects with problems in detection or photometry (close or inside the PC, partially out of field,...), and also those showing position angles outside the range $\pm 45^\circ$ from the predicted local shear. The final catalog contains 73 objects in A2218 and 81 objects in A370, the number of objects excluded by weak shear constraints being 2 and 12 respectively.

3.2. Absolute number counts

The observed and predicted number counts of arclets versus R magnitude in A2218 are shown in Figure 6. The predicted total number of arcs ($R_{F702W} \leq 23.5$ and $a/b \geq 2$) with the best mass model is lower than the observed number by a factor of 2 (table 3). Similar counts in A370 with $R_{F675W} \leq 23.5$ and $a/b \geq 2$ are displayed in Figure 7. Again, the models underpredict the observed counts by a factor of ~ 1.3 at the faintest magnitudes. The contamination by cluster members is possible, especially for the less elongated objects or the faintest ones. The number of objects excluded in each cluster allows to estimate this source of contamination, which is unable to explain all the observed excess. Some clues to understand this discrepancy in terms of cosmological parameters, LF and clustering are given in §4.

3.3. Color distributions

Another test of reliability for these results is to compare the predicted with the expected color distribution of arclets. To do that, the evolution with z of the color index $B - F702W$ was computed for the four morphological types of galaxy included in the model. Then, these dis-

Table 3. Comparison of different mass models for A2218 from Kneib et al. 1995 and Kneib et al. 1996. Number of arclets with $R \leq 23.5$ and $\mu_R \leq 25.5$ in the frame of the HST image for model 2a, compared to the observations.

| mass model | $a/b \geq 2$ | $a/b \geq 3$ |
|--------------------------------|--------------|--------------|
| bimodal (Kneib et al. 1995) | 12.1 | 5.1 |
| multimodal (Kneib et al. 1996) | 16.7 | 7.9 |
| observed arclets | 30 | 13 |

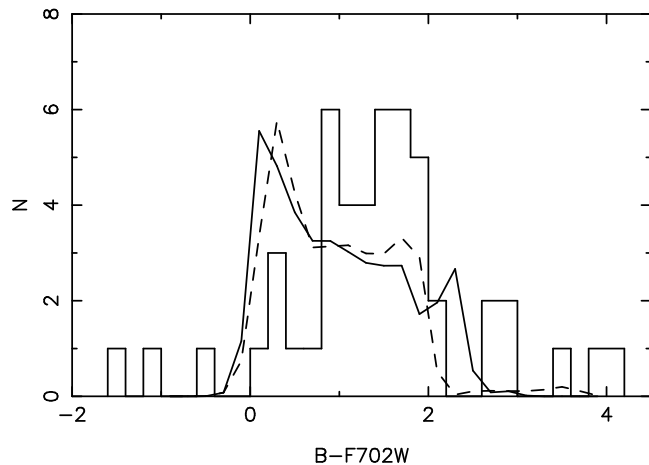


Fig. 8. Color distribution of arclets in A2218 with $R_{F702W} < 25.5$ and $a/b > 2$ (mass modelling by Kneib et al. (1996)) for model 1a (dashed line) and model 2a (solid line). The histogram is the observed color distribution.

crete values were replaced by a gaussian distribution for each type ($\sigma = 0.15$ mag.) and the counts in color were computed in the usual way. These predictions have been compared to the observed values in A2218. Because of the different detection conditions in the B -band compared to the WFPC2 (exposure time, seeing, pixel size), the resulting catalogue is limited to 49 objects with $B < 27.0$ and $a/b > 2$, 21 of them at $B < 24.5$. The color distribution of arclets in A2218 for $R_{F702W} \leq 25.5$ and $a/b \geq 2$ is shown in Figure 8. The observed range of $B - F702W$ is well reproduced by the models, although the modelled colors tend to be slightly bluer than observed. This effect is probably due to the way color indices are computed on CCD images: with such different sampling and observing conditions, colors are obtained roughly as the difference between the measured magnitudes, HST magnitudes being total ones while B -magnitudes are isophotal. As isophotal magnitudes tend to be overestimated at faint fluxes, the net effect is an artificial reddening of the sample which could explain this small discrepancy.

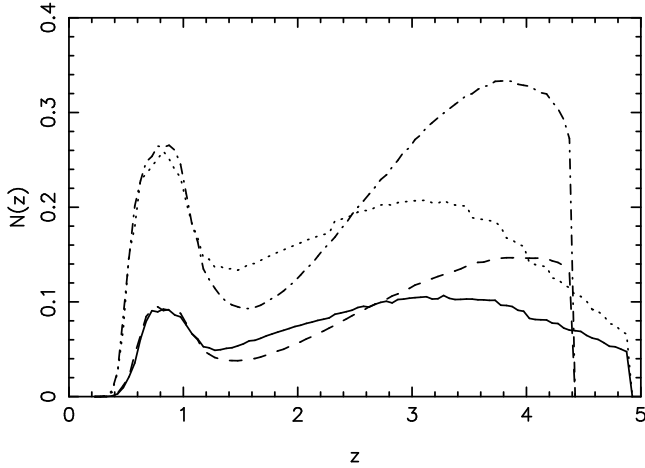


Fig. 9. Redshift distribution of arclets in A2218 per bin of 0.05 in z , in the HST field ($R_{F702W} \leq 23.5$ and $\mu_R \leq 24$) for $q_0 = 0$ (dot-dashed line: $a/b > 2$, dashed line: $a/b > 3$) or $q_0 = 0.5$ (dotted line: $a/b > 2$, solid line: $a/b > 3$).

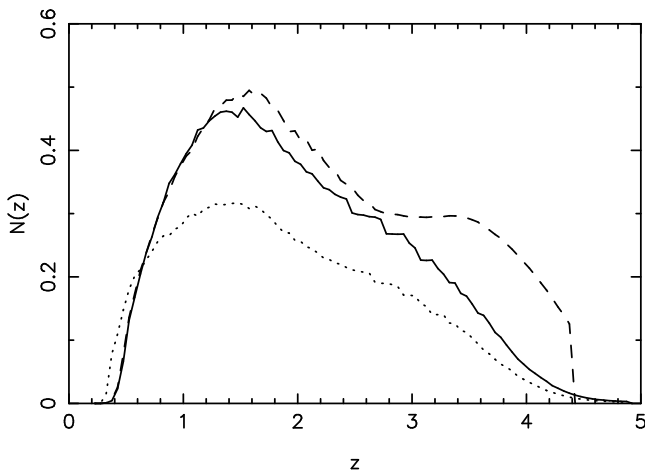


Fig. 10. Redshift distribution of arclets in A2218 per bin of 0.05 in z , with $B \leq 24.5$ and $a/b \geq 2$, according to the mass distribution by Kneib et al. (1996) for model 1a (dashed line) and model 2a (solid line). Dotted line corresponds to the bimodal mass distribution of Kneib et al. (1995) for model 2a. The cut at $z = 4.5$ corresponds to the redshift of formation for $q_0 = 0$.

3.4. Redshift distributions

For a direct comparison with existing deep redshift surveys, the redshift distribution of arclets has been computed in both B and R filters. These results are shown in Figures 9 and 10 for A2218, and in Figure 11 for A370. In the case of A2218, our results can be partially compared to the results of a successful spectroscopic survey of arclets (Ebbels et al. 1997), where 19 redshifts were obtained ranging from $z = 0.45$ to 2.5, and observed magnitudes from $R = 20.0$ to $R = 23.5$. This observed distribution peaks to a mean value of $\langle z \rangle = 0.7$, with

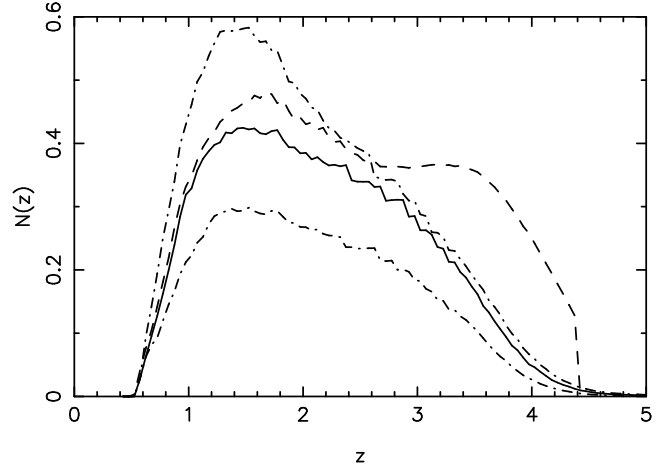


Fig. 11. Redshift distribution of arclets in A370 per bin of 0.05 in z ($B \leq 24.5$ and $a/b \geq 2$) for model 1a (dashed line) and model 2a (solid line). The dependence on the potential slope is shown as dot-dashed lines for $\gamma=1.1$ (upper line) and $\gamma=0.8$ (lower line) for model 2a. The cut at $z = 4.5$ corresponds to the redshift of formation for $q_0 = 0$.

only two objects at $z > 1$. Figure 9 shows the redshift distribution of arclets expected with the same selection conditions than that adopted by Ebbels et al. 1997. The peak observed is remarkably well reproduced. However, another population of objects is expected at higher redshifts, $z > 2$, with models 1 and 2, which is not seen in these data. This high redshift tail is mainly produced by E type galaxies and it is extremely sensitive to the redshift of formation assumed for the sources and to the hypothesis of no-evolution in morphological types. The maximum value of $N(z)$ at $z > 2$ is lowered by 30 – 50% assuming a redshift of formation $z_f \sim 6$, but the distribution extends to higher redshifts keeping the total number of objects approximately constant. Selection biases affecting the spectroscopic sample, the accuracy of the lens model and the effects of clustering behind the lens are discussed below (§4).

We have also tried to compare our model with a larger sample of giant arcs and arclets originating from different clusters (Figure 13), from a compilation of all measured redshifts at the present day. Again, in this sample arclets are mostly found between $z=0.5$ and 1, although arcs produced by different mass distributions are mixed and cannot be used for a close comparison with Figure 10. This sample is however interesting because it corresponds to arcs with high magnifications so the integrated flux favours the acquisition of better S/N ratio on the continuum of the spectra. Some absorption lines are expected to be observed at least in a few cases of star forming galaxies, and they would help in principle to determine redshifts in the range $1.2 \leq z \leq 2.2$ where no emission lines are present in the visible spectrum. This may be the case for the giant arc in Cl0024+17 (Mellier et al. 1991) where a

blue continuum is detected with no emission lines, but no firm identification has been proposed up to now. Being aware that objects with $1.2 \leq z \leq 2.2$ are systematically missed in spectroscopic surveys because of the lack of strong spectral features in their visible spectrum, we find again a similar trend: present-day arcs spectroscopy reveals very few objects at $z > 2$, whatever the selection criteria are.

3.5. Size evolution of sources

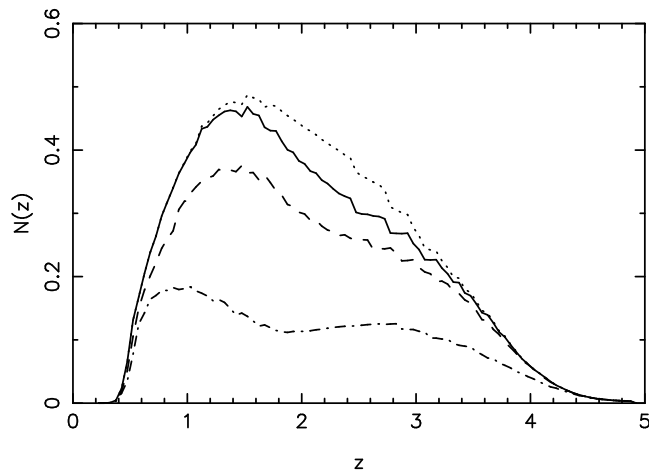


Fig. 12. Redshift distribution of arclets in A2218 per bin of 0.05 in z ($B \leq 24.5$, $a/b \geq 2$ and $\mu_B^0 \leq 26.5$). Solid line is for no seeing, dashed line corresponds to a seeing of $1''$ while dotted line corresponds to no seeing and no threshold in surface brightness, all curves are for model 2a. Dot-dashed line corresponds to model 2b with a seeing of $1''$ (evolution of the source size).

When neither the seeing nor the surface brightness are considered, the total number counts and the color distributions of arclets are almost independent of the size evolution of sources with redshift. On the contrary, when realistic ground-based detection conditions are introduced in the model, the resulting redshift distribution can differ significantly. Figure 12 shows these effects on the redshift distribution of arclets in A2218. When an atmospheric seeing of $1''$ is introduced together with size evolution of galaxies, the observed population splits into two components: one corresponds to spirals at redshifts of the order of 1 and the other one to ellipticals at z greater than 2. The former probably constitutes the bulk of the redshifts compiled in Figure 13 because most of these arcs were selected on ground based images and display emission lines. As expected, including an evolution of the size of galaxies does not change the results on HST data where the PSF is always smaller than the angular size of the sources whatever the redshift.

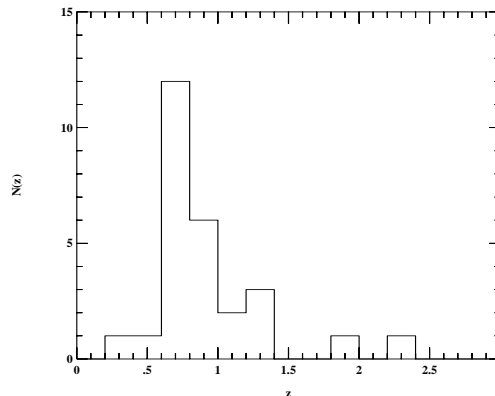


Fig. 13. Redshift distribution of arclets in several clusters except A2218. References: Soucail et al. 1988 (A370), Mellier et al. 1991 (A370 and Cl2244-02), Fort and Mellier 1994 (A2163 and S295), Pelló et al. 1991 (A2390), Bézecourt and Soucail 1997 (A2390), Melnick et al. 1993 (Cl2236-04), Kneib et al. 1994b (Cl2236-04), Smail et al. 1995 (AC114), Ellis et al. 1991 (A963), Lavery et al. 1993 (GHO2154+0508), Allen et al. 96 (PKS0745).

3.6. Optimisation of the search for high- z galaxies

One of the most interesting issues of this work is to produce a tool to select lensed galaxies at various redshifts. Instead of computing counts in the whole field, one can compute the 2D distribution for both counts and mean redshifts, in order to estimate and to compare the local densities all over the field. For computational reasons, the surface brightness distribution in §2.1.3 was replaced by the mean value of μ_B^0 for each morphological type. The results for A2218 are shown in Figure 14. The area where arclets are observed is fairly well identified (see Figure 1 in Kneib et al. 1996 for comparison). These figures show the places where the numerous high redshift objects (seen in the $N(z)$ curves) are expected. As one goes away from the cluster center, only arcs with high z can be lensed to acquire an axis ratio greater than 3. However, in the limiting area where arcs can be found, the cutoff in the density of arcs is quite sharp. In the very center of the cluster, radial arcs at high redshift are also predicted by the model. These objects remain unobserved because of obscuration by the cD envelope.

With the help of our model and maps similar to those in Figure 14 we can optimize the search for well defined samples of arclets and/or the search for high redshift lensed galaxies. The selection procedure could even benefit from the combination with redshifts estimated through multi-color photometric techniques (Pelló et al. 1996) or with the so-called “lensing redshift” (Kneib et al. 1994a, Kneib et al. 1996). Note that some high- z lensed galaxies at $z \geq 4$ have already been detected, although serendip-

itously, in the cluster Cl0949+4713 (Trager et al. 1997), or in Cl1358+62 (Franx et al. 1997), all of them showing "red" colors in the visible. This seems to indicate that, in the absence of a large wavelength coverage, the selection will have to rely on morphological information first and not on the usual criterium based on blue colors.

4. Discussion

The observed absolute number counts of arclets presented in Figures 6 and 7 tend to be overestimated with respect to the predicted values, especially at faint magnitudes where the excess attains a factor of 1.3 to 2, depending on the cluster. It is worth noting that computing number counts is difficult because of the large number of uncertainties involved in models, and some of them concerning the evolution of galaxies are quite similar to those encountered in empty fields. Firstly, counts in cluster lenses depend on the local normalisation of the LF, which has an uncertainty of a factor of 2 (see the discussion in Ellis et al. 1996), partly due to the statistical fluctuations from field to field and to the clustering of background galaxies. Secondly, as we are looking deeply in only a few lines of sight, these fluctuations may introduce a bias because the cluster-lenses selected at first are among those with the highest number of arcs and arclets. This particular bias is difficult to avoid, but it is not expected to induce a difference larger than a factor of 2 in the case of A2218, where the differences between observed and predicted number counts are the highest. A possible excess of galaxies at $z \simeq 0.45$ is already mentioned by Ebbels et al. (1997) but it does not seem to strongly distort the final redshift distribution. An example of clustering of background galaxies is observed behind another cluster-lens, namely the system of arclets in A2390 where two redshift planes are suspected behind the cluster (Bézecourt and Soucail 1997) preventing to do this kind of analysis.

Anyhow, a spectacular change in the number counts is obtained when we take into account the effects due to galaxy-scale mass components. The number of lensed objects is increased thanks to both the local increased magnification and the additional critical lines which divide giant arcs in smaller ones. A piece of evidence for this effect is given in §3.2 and §3.4 in the case of A2218, where the number of arclets is a factor of 1.5 higher when galaxy-scale mass components are introduced (Kneib et al. 1996). This is a strong justification of the need for accurate modelling when computing arcs statistics, and in this sense the present model is a clear improvement with respect to other previous similar works (Nemiroff and Dekel 1989, Grossman and Saha 1994). In particular, the absolute normalisation of counts through a cluster-lens is approached in a reliable way for A2218. In the case of A370, we plan to improve the lens modelling by adding the local effects of individual galaxies as additional mass components, thanks to the constraints given by new

spectroscopic results which clearly confirm some multiple image candidates (Bézecourt et al. in preparation). If the results are similar to those found in A2218 as expected, this procedure may reconcile the observed number of arclets presently in excess with model predictions for this cluster.

Another major point to discuss is the sensitivity of our results to the geometry of the universe. The two models considered here have been fixed to reproduce both number counts and redshift distributions of galaxies in the field. The mass models used in all the simulations were determined for a universe with $\Lambda = 0$ and $\Omega = 1$. It was assumed here that the same models were still valid for $\Omega = 0$ because varying Ω would not change the mass distributions by more than a few percents. This remark can also be extended to the value of Λ , which has a negligible effect on the lens-model parameters (less than 10%), but a more significant impact on the expected distribution of background sources. As shown in Figures 9 and 10, the value chosen for q_0 affects the expected distribution of background sources at high redshift. The total number counts are also sensitive to q_0 (Figures 9 and 10), especially at faint magnitudes where the main contribution comes from the more distant objects. Roughly speaking, when q_0 changes from 0.5 to 0 keeping $\Lambda = 0$, the efficiency of the cluster-lens given by $N(z)$ increases by a small factor of less than $\sim 10\%$ up to $z \sim 3$, but it rises dramatically up to a factor of $\sim 200\%$ at the highest z (Figures 6 and 7). The maximum effect on absolute number counts is $\sim 30\%$ for the faintest bins in magnitude ($B \sim 27 - 28$). When we change from a matter dominated ($(q_0, \lambda_0) = (0.5, 0.0)$) to a Λ dominated geometry ($(q_0, \lambda_0) = (0.0, 0.5)$) keeping $\Omega = 1$ ($\Omega = 2q_0 + 2\lambda_0$), the predicted number counts of arcs will increase by a 15% even at moderate magnitudes ($B = 24 - 25$). According to this result, models with $\lambda_0 \geq 0$ could reconcile observed with predicted number counts of arcs. The increase in number counts is even higher when we consider models with low values of Ω : it attains 40% at the same moderate magnitudes with $\lambda_0 \sim 0.9$ and $q_0 \leq 0$, but this model is somewhat unrealistic.

The main discrepancy between predicted and observed $N(z)$ for arclets is the apparent lack of objects observed at $z \geq 1$. Several arguments can be proposed to account for these missing galaxies: (a) a systematic bias in the sample of arclets selected for spectroscopy and/or in the successful sub-sample, (b) lens modelling is not accurate enough, and (c) the spectro-morphological properties of galaxies above $z \simeq 1$ are not well represented by the evolutionary models adopted here.

(a) Objects with z between about 1.2 and 2.2 can be missed in spectroscopic surveys because of the lack of any emission lines in the visible part of the spectrum. In the spectroscopic sample of Ebbels et al. (1997), it is striking that all the redshift determinations considered as secure correspond to spectra with an emission line, generally identified with [OII]. This clearly indicates a bias in the

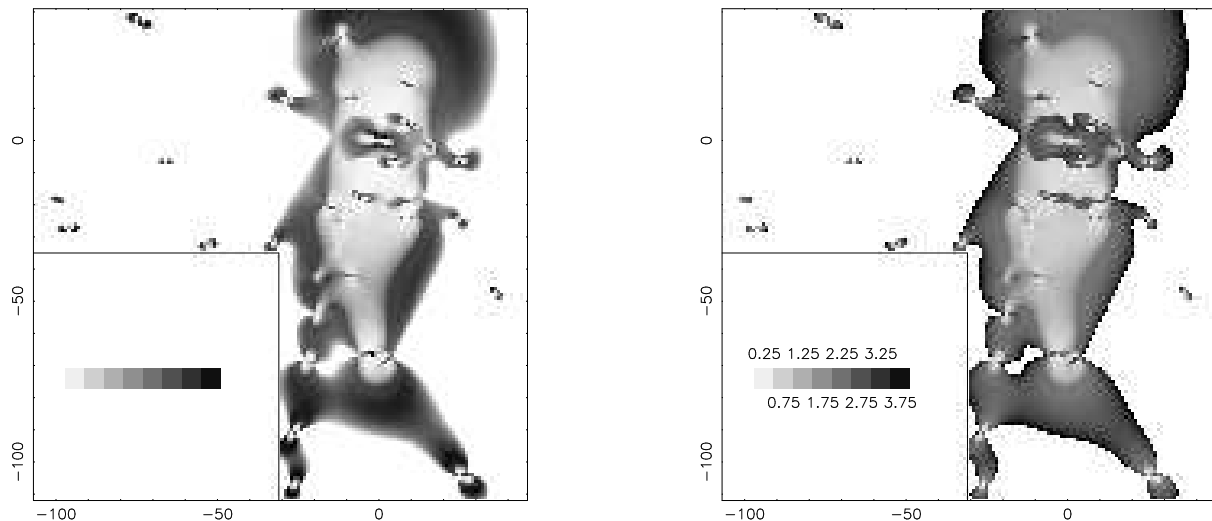


Fig. 14. Left: Density of arclets in cluster A2218 with $B < 24.5$ and $a/b > 3$ for model 1a. The arclets density increases from white pixels (null density) to black pixels. Right: Mean redshift of arclets in cluster A2218 with $B < 24.5$ and $a/b > 3$ for model 1a. Gray scale levels corresponds to redshift bins of $\Delta z = 0.5$ from $[0.0, 0.5]$ (clearer pixels) to $[3.5, 4.0]$ (black pixels).

spectroscopic sample to redshifts lower than 1.2 or higher than 2.2. About 40% of this sample of arclets remains with no redshift determination and may correspond to galaxies at $z > 1$. A more detailed examination of their photometric SEDs might allow to deduce a photometric redshift and to discuss this particular point. Anyway, as far as no well defined and magnitude-limited samples of arclets are studied yet, no direct comparison with our work can be proposed.

(b) Sensitivity to the lens mass distribution has been investigated by several methods, and we have shown that only minor effects apply on the redshift distribution when we change the main parameters of the lens models such as the core radius, the velocity dispersion or the slope of the potential, although this can significantly change the total number of lensed objects.

(c) Several uncertainties remain in the general problem of modelling galaxy evolution which could modify the predicted $N(z)$. Computing the redshift distribution of gravitational arclets with $B \leq 24.5$ is in fact equivalent to the distribution of field galaxies up to $B \simeq 26 - 26.5$ or fainter after magnification by the cluster. As the evolution model is constrained roughly until to $B = 24$, where spectroscopic data for field galaxies are available (Glazebrook et al. 1995, Cowie et al. 1996), a discrepancy may appear at fainter levels. Hence, we would meet here once more the excess in the number of high- z objects initially found in works about numbers counts (Bruzual and Kron 1980, Tinsley 1980, Guiderdoni and Rocca-Volmerange 1990, Metcalfe et al. 1991). It should be noted that the intro-

duction of internal absorption by dust in the model could decrease the counts at high redshift as we are mostly interested by the B -band, equivalent to the rest frame UV -band, where absorption effects are more important. This hypothesis has been explored by Campos and Shanks (1995). Metallicity effects are not taken into account here (metallicity is assumed to be solar), and would act in the opposite way because the UV luminosity is increased for a lower metallicity (as expected at earlier epochs).

The last point to comment is the difference found in the $N(z)$ distributions behind the two clusters. The fraction of galaxies at $z < 1$ is quite small in the case of A370 with respect to the high redshift tail. This is essentially related to the difference in the redshift of the lens: the magnification of galaxies at $z < 0.6$ is much less efficient in A370 ($z_{lens} = 0.37$) than in A2218 ($z_{lens} = 0.17$). This is also visible in the spectroscopic redshift survey of A2218 where 50% of the redshifts are smaller than 0.6.

5. Conclusions

We have shown that detailed absolute number counts, color and redshift distributions can be computed for lensed galaxies through an accurate modelling of the cluster-lens mass distribution. The framework for galaxy evolution has been chosen to fairly reproduce the observed number counts and redshift distribution of field galaxies. The interest in applying these calculations to arclets is to use cluster-lenses as filters to select faint distant galaxies. We have applied this procedure to two different cluster-lenses, A2218 and A370, for which the mass distribution is fairly

well known, and we have studied the impact of the different sources of uncertainty on the predicted number counts and redshift distributions, taking into account the observational conditions. The main result is that arcs at redshifts between 0.5 and 1 are correctly predicted by the modelling as observed. Nevertheless, an important population of high redshift arclets ($z \geq 1.0$) is also revealed by the simulations, which is not observed in spectroscopic surveys of arclets. This disagreement could result partly from a bias in the spectroscopy of arclets, but the main contribution is probably due to uncertainties in the evolutionary models for galaxies at high redshift.

In summary, our results show that a detailed model for the cluster-lens, including galaxy-scale mass components, is absolutely needed to interpret the observed distribution of arcs and arclets in terms of general properties of the background population of galaxies. A good agreement between model and observed absolute number counts can be obtained by a fine tuning parametrization of the evolutionary models for galaxies and/or the cosmological parameters. In this respect, the present work joins the problems encountered in the modelling of faint field galaxy samples (PBZ, Rocca-Volmerange and Guiderdoni 1990). Nevertheless, the difference in this case is that we are selecting high redshift galaxies and rejecting the faint neighbouring population. As evolutionary effects are extremely sensitive to the behaviour of sources at high redshift, the more distant the lens is, easier it will be to constrain them, provided one is able to detect a cluster lens with a sufficient number of arclets. In a more prospective way, observing distant cluster-lenses could help on disentangle the role of pure geometrical effects, giving constraints on the world model, from pure spectromorphological evolution. In any case, the piece of work presented here is just the beginning of a study, an example on two single clusters at moderate redshift, but the effort has to be pursued on a complete sample of lenses in order to minimize the fluctuations and possible clustering along the line of sight, which is difficult to avoid. For this reason, it is essential to define a homogeneous sample of cluster-lenses in order to derive reliable constraints on the absolute number of background galaxies. This could be explored by using the sample of distant clusters selected from the EMSS catalog (Gioia and Luppino 1994), but it would require an analysis of HST images for each cluster combined with an accurate modelling for all those identified as cluster-lenses.

Another interesting effect which is amplified when selecting high redshift objects is the role of elliptical galaxies. They are responsible for the bulk of the presently undetected population of high redshift arclets at $z \geq 2$. Changing the redshift of formation modifies the expected $N(z)$ distribution at such redshifts, but it does not reduce significantly the total excess in number. The most straightforward way to solve the problem is to break down the hypothesis that ellipticals form in a unique burst. This idea is also supported by the deep HST images (see also a

discussion in Baugh et al. 1997), where the distant galaxies seem rather irregular, deviating from the pure elliptical shape assumed here. In a more general way, there is no observational reason to assert that the progenitors of present day galaxies follow the simple evolutionary law used here (spectrophotometric evolution + $(1+z)^4$ dimming in surface brightness), and the first results on the arclet sample strongly support this idea. There is more probably a strong relationship between morphology and spectrophotometry, the two aspects being both interdependent and wavelength dependent. In any case, the identification of the distant progenitors of ellipticals remains an exciting challenge.

Computing the 2D distributions in number counts or mean redshift seems to be an important tool to build up independent samples of high redshift galaxies. We propose to couple together the computational tool presented here with photometric redshift techniques in order to select the spectroscopic samples. It is worth noting that arcs and arclets correspond to a sample of galaxies much less affected by biases in intrinsic luminosity. Besides, the brightest galaxies at any (high) redshift will be seen through lens magnification before being detected somewhere else.

Acknowledgements. We thank P'tit Lu Van Waerbeke, JP. Kneib, Y. Mellier, G. Bruzual and B. Fort for useful discussions and helpful comments. This work was partly supported by the Groupe de Recherche Cosmologie and by the French Centre National de la Recherche Scientifique.

References

- Allen S.W., Fabian A.C., Kneib J.-P., 1996, MNRAS, 279, 615
- Bartelmann M., Steinmetz M., Weiss A., 1995, A&A, 297, 1
- Baugh C.M., Cole S., Frenk C.S., Lacey C.G., 1997, preprint astro-ph/9703111
- Bertin E. & Arnouts S., 1996, A&AS, 117, 393
- Bézecourt J. & Soucail G., 1997, A&A, 317, 661
- Broadhurst T.J., Ellis R.S. and Glazebrook K. 1992, Nature, 355, 55
- Broadhurst T.J., 1995, preprint astro-ph/9511150
- Bruzual A.G. & Kron R.G., 1980, ApJ, 241, 25
- Bruzual G.A. & Charlot S., 1993, ApJ, 405, 538
- Campos A. & Shanks T., 1995, preprint astro-ph/9511110
- Cowie L.L., Songaila A., Hu E.M., Cohen J.G., 1996, AJ, 112, 839
- Crampton D., Le Fèvre O., Lilly S.J., Hammer F., 1995, ApJ, 455, 96
- Ebbels T.M.D., Le Borgne J.F., Pelló R., Kneib J.-P., Smail I.R., Sanahuja B., 1996, MNRAS 281, L75
- Ebbels T.M.D., Ellis, R.S., Kneib J.-P., Le Borgne J.F., Pelló R., Smail I.R., Sanahuja B., 1997, MNRAS submitted, SISSA preprint astro-ph/9703169
- Efstathiou G., Ellis R.S., Peterson B.A., 1988, MNRAS, 232, 431
- Ellis R.S., 1997, ARAA, 35, in press
- Ellis R.S., Allington-Smith J., Smail I., 1991, MNRAS, 249, 184

- Ellis R.S., Colless M., Broadhurst T., Heyl J., Glazebrook K., 1996, MNRAS, 280, 235
- Fort B. & Mellier Y., 1994, A&AR, 5, 239
- Fort B., Mellier Y., Dantel-Fort M., 1996, A&A, 321, 353
- Franx M., Illingworth G.D., Kelson D.D., van Dokkum P.G., Tran K-V., 1997. preprint astro-ph/9704090
- Frye B., & Broadhurst T., 1997, ApJ Letters in preparation
- Fukugita M., Shimasaku K., Ichikawa T. 1995, PASP 716, 945
- Gioia I.M. & Luppino G.A., 1994, ApJS 94, 583
- Glazebrook K., Ellis R., Colless M., Broadhurst T., Allington-Smith J., Tanvir N., 1995, MNRAS, 273, 157
- Grossman S.A. & Saha P., 1994, ApJ 431, 74
- Guiderdoni B. & Rocca-Volmerange B., 1990, A&A, 227, 362
- Hammer F., 1991, ApJ, 383, 66
- Hattori M., Watanabe K., Yamashita K., 1997, A&A, 319, 764
- Kassiola A. & Kovner I., 1993, ApJ 417, 450
- King I.R., 1978, ApJ, 222, 1
- Kneib J.-P., Mellier Y., Fort B., Mathez G., 1993, A&A, 273, 367
- Kneib J.-P., Mathez G., Fort B., Mellier Y., Soucaïl G., Longaretti P.-Y., 1994a, A&A, 286, 701
- Kneib J.-P., Melnick J., Gopal-Krishna, 1994b, A&A, 290, L25
- Kneib J.-P., Mellier Y., Pelló R., Miralda-Escudé J., Le Borgne J.F., Böhringer H., Picat J.-P., 1995, A&A, 303, 27
- Kneib J.-P., Ellis R.S., Smail I., Couch W.J., Sharples R.M., 1996, ApJ, 471, 643
- Koo D.C. & Kron R.G., 1992, ARAA, 30, 613
- Kruit P.C. van der, 1987, A&A, 173, 59
- Lavery R.J., Pierce M.J., McClure R.D., 1993, ApJ, 418, 43
- Le Borgne J.-F., Pelló R., Sanahuja B., 1992, A&AS, 95, 87
- Lilly S.J., Tresse L., Hammer F., Crampton D., Le Fèvre O., 1995, ApJ, 455, 108
- Lowenthal J.D., Koo D.C., Guzmán R., Gallego J., Phillips A.C., Faber S.M., Vogt N.P., Illingworth G.D., Gronwall C., 1997, ApJ 481, 673
- Mathewson D.S., Ford V.L., Buchhorn M., 1992, ApJS, 81, 413
- Mellier Y., Soucaïl G., Fort B., Mathez G., 1988, A&A, 199,13
- Mellier Y., Fort B., Soucaïl G., Mathez G. and Cailloux M., 1991, Ap.J., 380, 334
- Melnick J., Altieri B., Gopal-Krishna, Giraud E., 1993, A&A, 271, L5
- Metcalfe N., Shanks T., Fong R., Jones L.R., 1991, MNRAS, 249, 498
- Mutz S.B., Windhorst R.A., Schmidtke P.C., Pascarelle S., Griffiths R.E., Ratnatunga K.U., Casertani S., Im M., Ellis R.S., Glazebrook K., Green R.F., Sarajedini V.L., 1994, ApJ, 434, L55
- Narayan R. & Bartelmann M., 1996, Lectures on gravitational lensing, Jerusalem
- Nemiroff R.J. & Dekel A., 1989, ApJ, 344, 51
- Pelló R., Le Borgne J.F., Soucaïl G., Mellier Y. and Sanahuja B., 1991, ApJ, 366, 405
- Pelló R., Le Borgne J.F., Sanahuja B., Mathez G., and Fort B., 1992, A&A, 266, 6
- Pelló R., Miralles J.M., Le Borgne J.F., Picat J.P., Soucaïl G., Bruzual G., 1996, A&A, 314, 73
- Pelló R., et al., 1997, A&A, in preparation
- Pozzetti L., Bruzual G.A., Zamorani G., 1996, MNRAS, 281, 953
- Refregier A. and Loeb A., 1997, ApJ, 478, 476
- Rocca-Volmerange B. & Guiderdoni B., 1990, MNRAS, 247, 166
- Salpeter E.E., 1955, ApJ, 121, 161
- Scalo J.M., 1986, Fund. Cosmic Phys., 11, 1
- Soucaïl G., Mellier Y., Fort B., Mathez G., Cailloux M., 1988, A&A, 191, L19
- Smail I., Ellis R.S., Fitchett M.J., Nørgaard-Nielsen H.U., Hansen L., Jørgensen H.E., MNRAS, 1991, 252, 19
- Smail I., Ellis R.S., Fitchett M.J., 1994, MNRAS, 270, 245
- Smail I., Couch W.J., Ellis R.S., Sharples R.M., 1995, ApJ, 440, 501
- Smail I., Dressler A., Kneib J.-P., Ellis R., Couch W.J., Sharples R.M., Oemler A., Butcher H.R., 1996, ApJ, 469, 508
- Tinsley B.M., 1980, ApJ, 241, 41
- Trager S.C., Faber S.M., Dressler A., Oemler A., 1997, ApJL in press, preprint astro-ph/9703062
- Williams R.E., Blacker B., Dickinson M., Van Dyke Dixon W., Ferguson H.C., Fruchter A.S., Giavalisco M., Gilliland R.L., Heyer I., Katsanis R., Levay Z., Lucas R.A., McElroy D.B., Petro L., Postman M., Adorf H.-M., Hook R.N., 1996, AJ, 112, 1335
- Wu X.P. & Hammer F., 1993, MNRAS, 262, 187